

# Magnetoelastic interactions in $\text{SrCu}_2(\text{BO}_3)_2$ studied by Raman scattering experiments and first principles calculations

K. Thirunavukkuarasu<sup>1</sup>, G. Radtke<sup>2</sup>, Z. Lu<sup>3</sup>, M. Lazzeri<sup>2</sup>, P. C. M. Christianen<sup>4</sup>, M. V. Ballottin<sup>4</sup>,  
H. A. Dabkowska<sup>5</sup>, B. D. Gaulin<sup>5</sup>, D. Smirnov<sup>6</sup>, M. Jaime<sup>6</sup>, and A. Saúl<sup>7,\*</sup>

<sup>1</sup>Department of Physics, Florida A & M University, 1530 South Martin Luther King Jr. Boulevard, Tallahassee, Florida 32307, USA

<sup>2</sup>Sorbonne Université, CNRS, MNHN, IRD, Institut de Minéralogie, de Physique des Matériaux, et de Cosmochimie (IMPMC),  
4 place Jussieu, 75252 Paris cedex 05, France

<sup>3</sup>National High Magnetic Field Laboratory, Florida State University, 1800 East Dirac Drive, Tallahassee, Florida 32310, USA

<sup>4</sup>High Field Magnet Laboratory (HFML-EMFL), Radboud University, Toernooiveld 7, 6525 ED Nijmegen, Netherlands

<sup>5</sup>McMaster University, Brockhouse Institute of Materials Research, Hamilton, Ontario L8S 4M1, Canada

<sup>6</sup>MPA-MAGLAB, Los Alamos National Laboratory, Los Alamos, New Mexico 87545, USA

<sup>7</sup>Aix-Marseille University, Centre Interdisciplinaire de Nanoscience de Marseille-CNRS (UMR 7325), Marseille, France



(Received 10 November 2022; accepted 24 January 2023; published 9 February 2023)

Dynamic and static crystal lattice properties of  $\text{SrCu}_2(\text{BO}_3)_2$  are studied by means of Raman scattering, magnetostriction, and thermal expansion measurements in magnetic fields to 45 T. Raman experiments versus temperature reveal that some phonon modes show an unusual behavior: their frequencies soften (modes at 200 and 450  $\text{cm}^{-1}$ ) while others harden (modes at 385 and 478  $\text{cm}^{-1}$ ) when decreasing the temperature below 15 K. Magneto-Raman experiments show that their field dependence correlates with their respective temperature dependencies; e.g., modes that are hardened with increasing temperature also harden with applied magnetic fields and modes that become softer with temperature also soften with applied fields. We use density functional theory to successfully model and compute the energies of these modes, classifying them into two types: pantograph (modes that soften when decreasing the temperature) and nonpantograph. We conclude that the former involves the modification of the intradimer exchange interaction  $J$  and the latter the interdimer  $J'$ . Finally, dilatometry is used to correlate field-dependent Raman modes to the closing of the spin gap as well as fractional-magnetization stripe states  $M = 1/4 M_s$  and  $M = 1/3 M_s$ , where  $M_s$  is the saturation magnetization.

DOI: [10.1103/PhysRevB.107.064410](https://doi.org/10.1103/PhysRevB.107.064410)

## I. INTRODUCTION

$\text{SrCu}_2(\text{BO}_3)_2$  is a Mott-Hubbard insulator that hosts an orthogonal spin-dimer system, with a tetragonal unit cell that accommodates spin  $S = 1/2$   $\text{Cu}^{2+}$  dimers arranged in copper-oxygen-boron planes separated by strontium spacer layers as shown in Fig. 1.  $\text{SrCu}_2(\text{BO}_3)_2$  is also a physical realization of the two-dimensional Shastry-Sutherland model proposed more than four decades ago [1]. Here, oxygen-mediated magnetic superexchange results in an interdimer  $J'$  to intradimer  $J$  exchange constant ratio  $J'/J \simeq 0.63$ , that leads to an exact spin-singlet ground state, close to a critical point at  $J'/J \simeq 0.68$  marking a transition to an intermediate *plaquette* phase [2]. The combination of geometrical frustration, tunable exchange interactions that are sensitive to the  $\widehat{\text{CuOCu}}$  angle, and proximity to the critical point make this a fascinating compound, very rich in magnetic phases that have been predicted and observed to be stabilized with tuning parameters such as temperature, external magnetic fields, applied pressures, and disorder induced by minute chemical substitutions as attested by more than two decades of exciting research and results [3–16]. Indeed, it is known from extensive

earlier work that, when in the low-temperature spin-dimer ground state, applied magnetic fields, external pressure, and temperature have similar effects on the lattice properties and physics of  $\text{SrCu}_2(\text{BO}_3)_2$ . This, due to all three control parameters ultimately being responsible for the suppression of the spin-gapped state, makes  $\text{SrCu}_2(\text{BO}_3)_2$  a unique system for the numerous practical routes available to tune exotic states such as spin stripe phases, spin supersolids, plaquettes, and quantum spin liquids, just to mention a few.

Work by Radtke and collaborators [10] first identified and quantitatively demonstrated that an optically active lattice mode coined the *pantograph* mode is behind the strong spin-lattice coupling in  $\text{SrCu}_2(\text{BO}_3)_2$  amplifying the influence of minute lattice parameter variations via the  $\widehat{\text{CuOCu}}$  bond angle and resulting in an altered  $\text{Cu}^{2+} - \text{Cu}^{2+}$  exchange interaction that effectively stabilizes spin stripes and magnetization plateaus. Further work by Bettler *et al.* [18] has shown that the pantograph mode, which surprisingly softens with lowering temperatures, hardens under applied pressure to the point of changing its temperature dependence entirely with an external pressure of 27.5 kbar. These results are intriguing, because in more standard magnetic systems lattice modes often freeze and harden upon reducing the temperature.

Raman spectroscopy has been successfully used to probe lattice and spin degrees of freedom in  $\text{SrCu}_2(\text{BO}_3)_2$  [18–25]

\* andres.saul@cnrs.fr

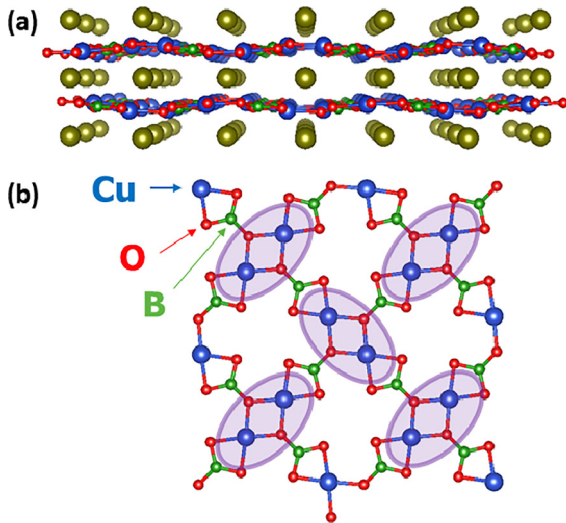


FIG. 1. Atomic structure of  $\text{SrCu}_2(\text{BO}_3)_2$  (a) along the  $[100]$  direction and (b) along the  $[001]$  direction. Sr atoms are in yellow, O in red, B in green, and Cu in blue. The buckling of the  $[\text{CuBO}_3]^-$  layers along the  $[001]$  direction is visible in (a). The orthogonal Cu dimers have been highlighted in magenta in (b). Atomic structures were drawn with VESTA [17].

including a recent study of low-energy magnetic excitations at high magnetic fields up to 27 T [26]. For further understanding the role of the lattice in stabilizing magnetic structures and exotic spin states, here we expand the range of magneto-Raman studies and trace the behavior of magnetic-field-dependent phonon modes up to 45 T. We use density functional theory to successfully compute the observed field-dependent Raman modes, classifying them into two types: *pantograph* and *nonpantograph* modes, and show that while the former are unusual, the latter display enhanced but more conventional temperature dependence. We also show that their field dependence correlates with their respective temperature dependencies; e.g., modes that are hardened with increasing temperature also harden with applied magnetic fields and modes that become softer with temperature also soften with applied fields and are, likely, going to be important in field- (or pressure-) induced states. The detailed evolution of the mode energies in magnetic fields mimic the changes observed in dilatometry and magnetization, displaying anomalies at plateaus. Last but not least, we observe via dilatometry that the coefficient of thermal expansion appear to vanish at magnetic fields in the proximity of the closing of the spin gap, a feature not entirely understood at the moment.

## II. EXPERIMENTAL DETAILS

High-quality single crystals of incongruently melting  $\text{SrCu}_2(\text{BO}_3)_2$  were grown by the optical floating zone technique in an image furnace using self-flux. Selected single crystals were oriented and characterized by x-ray diffraction and by neutron scattering using highly enriched  $^{11}\text{B}$  as described elsewhere; see Dabkowska *et al.* [27].

Raman spectroscopic experiments at high magnetic fields were performed using three different magnet systems. Two of the experimental facilities are the 45 T hybrid magnet and 31 T resistive magnet at the National High Magnetic

Field Laboratory (NHMFL) in Tallahassee, USA. The third Raman facility coupled to a 30 T resistive magnet is stationed at High Field Magnet Laboratory (HFML) in Nijmegen, Netherlands. The crystals were mounted in a custom-built fiber-based (NHMFL) or a direct-optics (HFML) probe inserted in a cryostat with helium exchange gas. Scattered light was collected in backscattering geometry from the  $ab$  plane of the  $\text{SrCu}_2(\text{BO}_3)_2$  crystal with the magnetic field applied along the  $c$  axis (Faraday geometry) using a 532 nm laser excitation focused to a (2–4)- $\mu\text{m}$ -diameter spot with incident power of about 100  $\mu\text{W}$  to minimize sample heating. The Raman spectra were analyzed by a monochromator (NHMFL: SP2750 Princeton Instruments, 1800 g/mm grating; HFML: Horiba FHR1000, 1200 g/mm grating) and recorded by a liquid-nitrogen-cooled CCD (PyLoN 100BR, Princeton Instruments) with a spectral resolution of about  $1\text{ cm}^{-1}$ . The magneto-Raman measurements were carried at lowest stable temperature of about 2 K. The temperature-dependent and polarization-resolved Raman spectra were collected using a direct beam optics setup (HFML).

High-field magnetostriction and thermal expansion measurements were performed using an optical fiber Bragg grating (FBG) technique in the NHMFL 45 T hybrid magnet at pumped  $^4\text{He}$  temperatures [28]. Axial dilatometry data,  $\Delta c/c(T, B)$ , were obtained as a function of the temperature and magnetic field to 45 T applied along the crystallographic  $c$  axis. The data were obtained with a swept wavelength laser interrogator by Micron Optics, yielding a resolution  $\Delta L/L = 3 \times 10^{-8}$ .

## III. COMPUTATION DETAILS

Density functional theory (DFT) calculations have been carried out using the pseudopotential plane-wave method as implemented in the QUANTUM ESPRESSO suite of codes [29]. The self-consistent electronic structure and the phonon modes and Raman spectra have been calculated using the PWscf and PHONON codes, respectively. In our calculations, we used optimized norm-conserving Vanderbilt (ONCV) pseudopotentials and the PBE functional [30] with a plane-wave and charge-density cutoff of 80 Ry and 320 Ry, respectively. We included an on-site Hubbard  $U_{\text{eff}}$  on the Cu atoms using the simplified method developed by Cococcioni and de Gironcoli [31] with a  $U_{\text{eff}} = 10.3\text{ eV}$ . The phonon band structure has been computed using the PHONOPY [32] code with a  $2 \times 2 \times 2$  supercell.

## IV. RESULTS

### A. Phonon modes and Raman spectra

The calculated phonon band structure and projected density of states are shown in Fig. 2. The high-energy modes above  $1150\text{ cm}^{-1}$  concern the B-O bonds. The flat band around  $920\text{ cm}^{-1}$  involves the in-plane movement of the three O atoms elongating or stretching the B-O bonds. The energy band between  $580$  and  $700\text{ cm}^{-1}$  also concerns the B-O bonds and in particular the out-of-plane movement of the B atoms on the top of the band. Finally, the modes below  $450\text{ cm}^{-1}$  involve the Cu-O bonds while the low-energy modes below  $100\text{ cm}^{-1}$  are mostly localized on the Sr atoms.

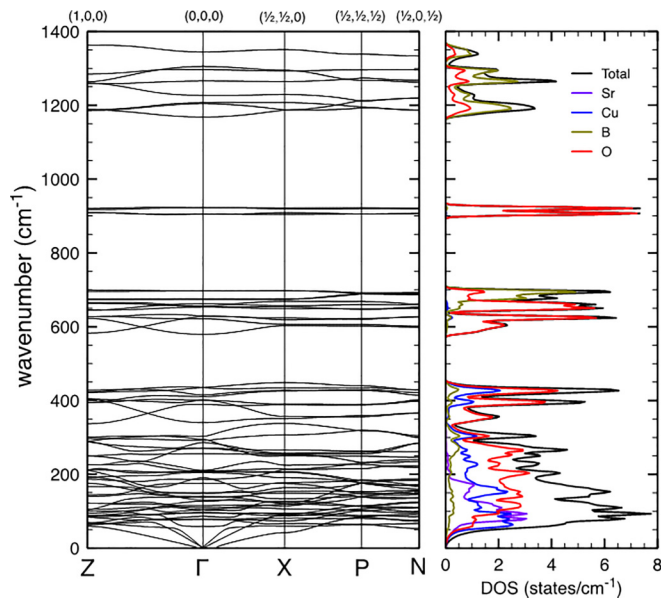


FIG. 2. Phonon band structure and projected density of states of  $\text{SrCu}_2(\text{BO}_3)_2$ .

Parallel and cross-polarized, (*aa*) and (*bb*), zero-field Raman spectra measured at 7 K are shown in Fig. 3(a). In the measured frequency range, our measurements are consistent with the previous studies [20,23]. In Fig. 3(b) we show the calculated spectra. There is an overall good agreement between the spectra apart from a stretch of 7% of the theoretical frequencies, which is state-of-the-art when comparing experimental and theoretical Raman spectra. In Fig. 3(a) we have labeled with their energy (200, 385, 450, and 478  $\text{cm}^{-1}$ ) the four experimental modes involving the Cu-O bonds, i.e., below 480  $\text{cm}^{-1}$  in the experimental spectra. In Fig. 3(b), we have used the same labels for the theoretical modes de-

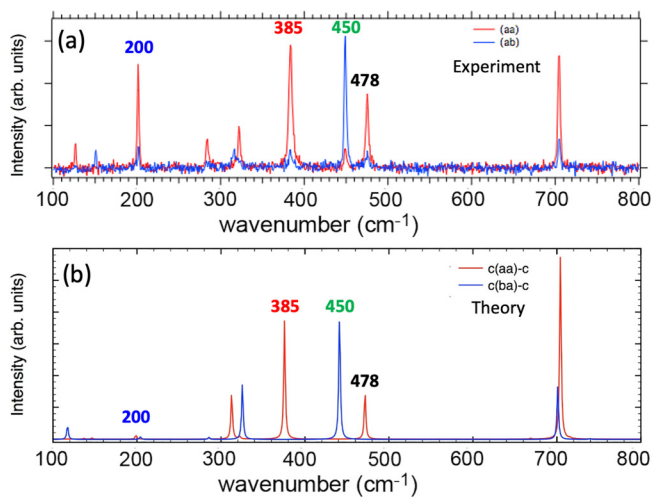


FIG. 3. Comparison of the (a) experimental spectra of  $\text{SrCu}_2(\text{BO}_3)_2$  measured at 7 K and (b) theoretical Raman spectra for two polarizations. The energy of the theoretical spectra has been stretched by 7%. The four intense experimental phonon modes involving Cu-O bonds whose schematic representation in Fig. 5 are labeled in the spectra (see text).

spite that their calculated frequencies are slightly different (189, 340, 415, and 434  $\text{cm}^{-1}$ ). The relative experimental intensities are fairly well reproduced by the theoretical calculations with the exception of the intensity of the mode at 200  $\text{cm}^{-1}$ .

### B. Temperature dependence

Raman spectra from the *ab* plane of  $\text{SrCu}_2(\text{BO}_3)_2$  were measured as a function of temperature in the range from 295 K to 2 K. To examine the Raman data, we fitted the relevant Raman peaks with Lorentzians and plot the extracted peak positions in Fig. 4(a). Typically for phonons in crystalline solids, the phonon frequencies are almost constant below cryogenic temperatures and exhibit a redshift with increasing temperature due to the combined effects of anharmonic phonon-phonon interaction and thermal expansion. We found that all measured  $\text{SrCu}_2(\text{BO}_3)_2$  phonon modes that do not involve the Cu-O bonds exhibit such usual temperature dependence in the whole measured temperature range. The phonon modes involving the Cu-O bonds behave quite differently at low temperatures showing spectacular deviations below 15 K. As summarized in Fig. 4(a), the frequencies of the phonons at 385  $\text{cm}^{-1}$  and 478  $\text{cm}^{-1}$  show quick upturn while the modes at 200  $\text{cm}^{-1}$  and 450  $\text{cm}^{-1}$  change in the opposite direction. Similar temperature dependence for phonons at 200  $\text{cm}^{-1}$  and 385  $\text{cm}^{-1}$  has been recently reported [26].

Our DFT calculations allowed us to analyze the four modes showing anomalous temperature dependence (see Fig. 5). The mode at 200  $\text{cm}^{-1}$  with the strongest temperature dependence is indeed the pantograph mode [2,10,18]. As can be seen, in this mode there is a rigid movement of the  $\text{CuBO}_3$  groups. The Cu-Cu intradimer distance oscillates and the O-O distance also oscillates but in antiphase. As a consequence these displacements involve a modification of the  $\widehat{\text{CuOCu}}$  superexchange angle [10]. The mode at 450  $\text{cm}^{-1}$  also shifts to higher energies when increasing temperature [see Fig. 4(a)]. The four  $\text{BO}_3$  groups around the Cu dimers move almost rigidly, but now the Cu atoms move in the opposite direction with respect to the  $\text{BO}_3$  group and their relative displacement is smaller. The relative displacement of the Cu and O atoms also involves a modification of the  $\widehat{\text{CuOCu}}$  superexchange angle. This appears as a signature for the modes whose energies soften with decreasing temperature. In contrast, as can be seen in Fig. 5, the modes at 385 and 478  $\text{cm}^{-1}$  whose frequencies rise when decreasing temperature do not involve a significant modification of the  $\widehat{\text{CuOCu}}$  superexchange angle. In particular in the 478  $\text{cm}^{-1}$  mode, the Cu and O displacements can be seen as an almost angle-preserving homothetic transformation of the  $\text{Cu}_2\text{O}_2$  plaquette (see Fig. 5). In the 385  $\text{cm}^{-1}$  mode, the only moving atoms are the oxygens of the  $\text{BO}_3$  groups that collectively rotate around the B atom.

### C. Magnetic field dependence

The four strongest modes involving the Cu-O bonds (200, 385, 450, and 478  $\text{cm}^{-1}$ ) that exhibit significant temperature dependence also show significant response to the external magnetic field. Figure 6(a) shows the magnetic field dependence of their energies at 2 K and magnetic fields up to 45 T. Figures 6(c) and 6(d) show waterfall plots with the evolution

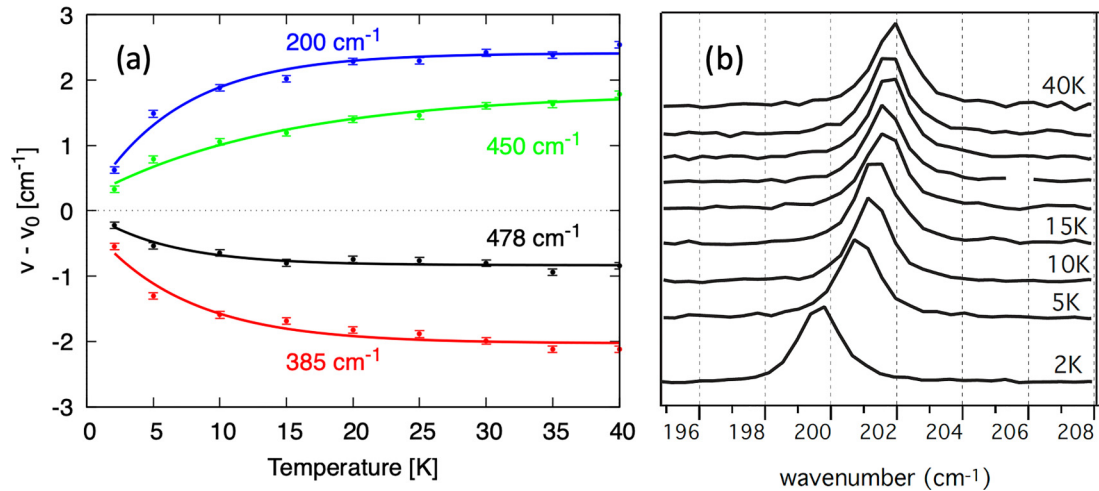


FIG. 4. (a) Evolution of the energy of four Raman modes of  $\text{SrCu}_2(\text{BO}_3)_2$  at  $B = 0$  with temperature and (b) waterfall plot showing the evolution of the energy of the peak at  $200 \text{ cm}^{-1}$  with temperature. In (a), the lines are exponential fits to the experimental points that extrapolate to zero at zero temperature. They must be considered as guides to the eye.

of the  $200 \text{ cm}^{-1}$  pantograph mode with the applied magnetic field in the range 24–44 T.

The overall change of the phonon modes with increasing magnetic field is similar to the shifts observed for increasing temperature. The energy of phonons at  $200 \text{ cm}^{-1}$  and  $450 \text{ cm}^{-1}$  shift to higher energies with increasing magnetic field while the energy of phonons at  $385 \text{ cm}^{-1}$  and  $478 \text{ cm}^{-1}$  lower their energies.

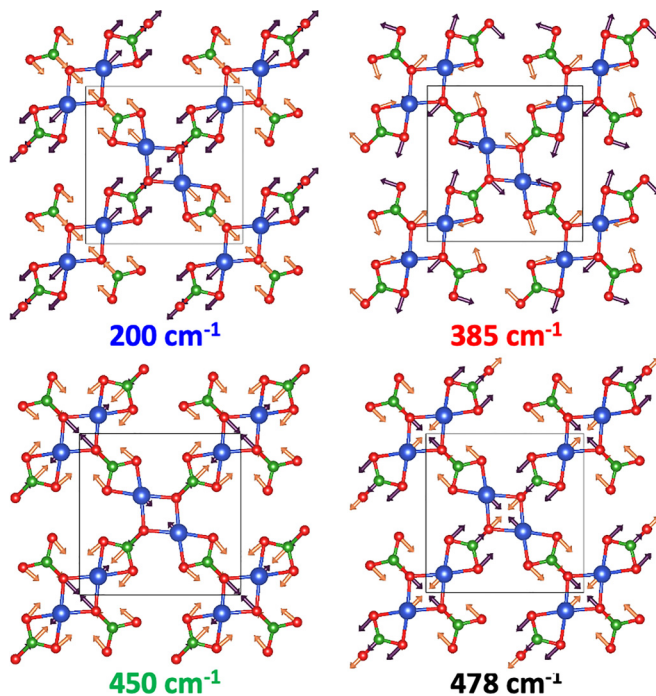


FIG. 5. Schematic representation of the phonon modes of  $\text{SrCu}_2(\text{BO}_3)_2$  with strongest temperature and magnetic field dependence. The lengths of the arrows are proportional to the atomic displacements. Phonon mode visualizations were drawn with VESTA [17]. Displacement diagrams labeled  $200 \text{ cm}^{-1}$  and  $450 \text{ cm}^{-1}$  show Cu and O atom motion consistent with the pantograph modes, while  $385 \text{ cm}^{-1}$  and  $478 \text{ cm}^{-1}$  are nonpantograph.

The observation of magnetic-field-induced response similar to temperature dependence suggests that the same magnetoelastic interactions are at play. The thermal excitations involve the same physical mechanisms as that of the magnetic excitations.

For the pantograph phonon modes at  $200 \text{ cm}^{-1}$  and  $450 \text{ cm}^{-1}$  the modification with temperature and magnetic field of the superexchange paths can be the mechanism at the origin of the observed hardening. When increasing temperature or applying a magnetic field, the spins localized in some Cu dimers would orient parallel to each other. As the interaction is AFM, the system would try to decrease the superexchange angle in order to decrease the interaction. The slight decrease of the angle is obtained by shortening the Cu-Cu distance [10] which leads to the hardening of the pantograph phonon modes [2].

Similar conclusions about the common origin of the temperature and magnetic field dependence can be drawn by comparing the macroscopic deformation of the lattice parameter measured in magnetostriction experiments [8,10] as shown in Figs. 6(b) and 7 and the corresponding deformation measured versus temperature in neutron scattering experiments [33].

We now discuss possible origins of magnetic field sensitivity of nonpantograph phonon modes. As mentioned above these modes do not involve a significant modification of the superexchange angle. In the  $478 \text{ cm}^{-1}$  mode, the Cu and O displacements concern an almost angle-preserving homothetic transformation of the  $\text{Cu}_2\text{O}_2$  plaquette and in the  $385 \text{ cm}^{-1}$  mode, the oxygens of the  $\text{BO}_3$  rotate around the B atom (see Fig. 5). The symmetry of their movement does not affect the intradimer interaction  $J$  but it does modify the second-neighbor interaction  $J'$ , which depends on the longer effective exchange path Cu-O-B-O-Cu. In particular, the homothetic transformation of the  $478 \text{ cm}^{-1}$  mode modifies both interactions  $J'$  connecting one Cu atom to a perpendicular dimer in a similar in-phase manner, while the rotation of the  $\text{BO}_3$  groups of the  $385 \text{ cm}^{-1}$  mode breaks the symmetry of the two  $J'$  interactions breaking the frustration of the ground state. This

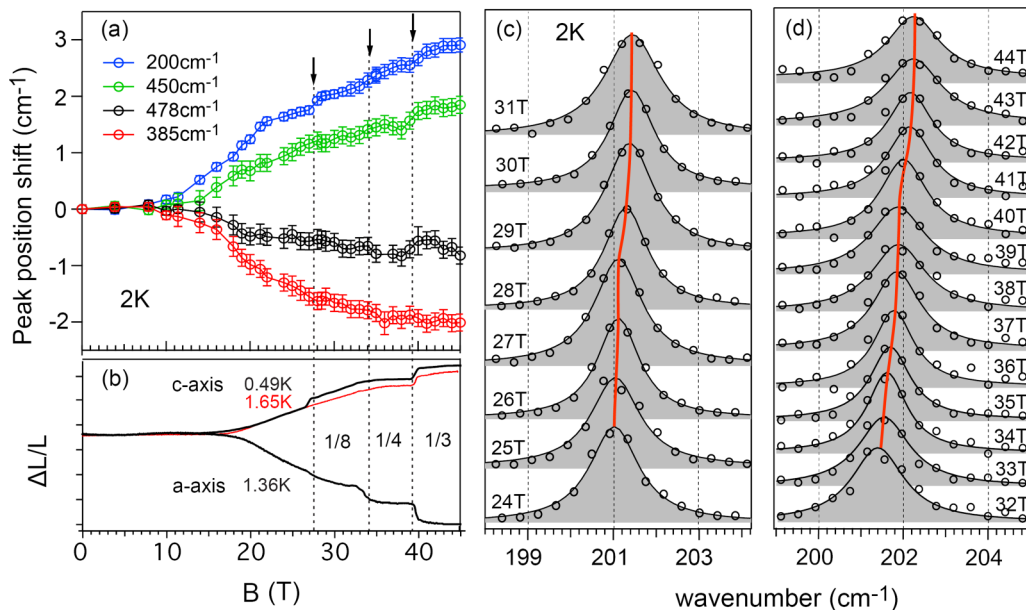


FIG. 6. (a) Evolution of the energy of four Raman modes of  $\text{SrCu}_2(\text{BO}_3)_2$  with applied magnetic fields up to 45 T. The arrows point to the anomalies detected in  $200 \text{ cm}^{-1}$  mode coinciding with  $M/M_s = 1/8, 1/4,$  and  $1/3$  phases. The energy of the modes was obtained from Lorentzian fit of the average spectrum over multiple spectra obtained at each magnetic field step. The error bars were obtained from the data deviation at each spectrum in the group. (b) Magnetostriction of  $\text{SrCu}_2(\text{BO}_3)_2$  along  $a$  and  $c$  crystallographic axes measured at magnetic fields up to 45 T. Adapted from Ref. [10]. (c) and (d) Evolution of the  $200 \text{ cm}^{-1}$  pantograph phonon mode with respect to increasing magnetic fields in the range 24–44 T. The data points are shown as open circles and the solid lines are the Lorentzian fit of the data.

is probably the reason explaining the enhanced temperature and magnetic field dependence for this last mode.

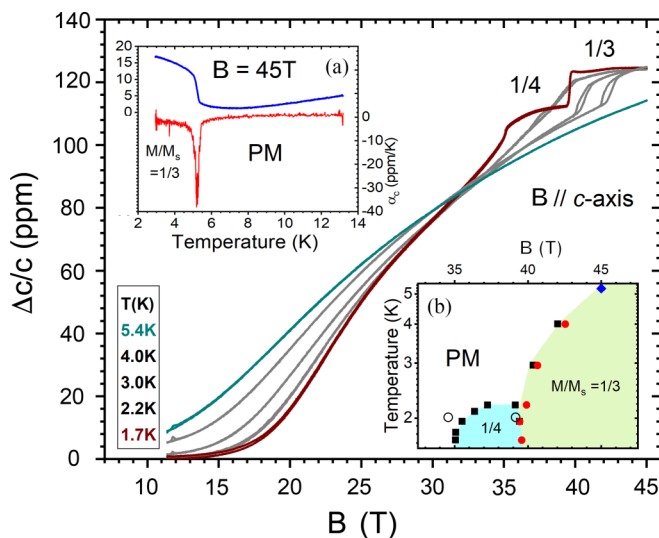


FIG. 7. Main panel:  $c$ -axis magnetostriction measured to 45 T at different temperatures between 1.7 K and 5.4 K. Inset (a): Thermal expansion  $\Delta c/c$  (left y axis) and coefficient of thermal expansion  $\alpha$  (right y axis) vs temperature measured at constant magnetic field  $B = 45 \text{ T}$ , showing a sharp phase transition at 5.2 K. Inset (b):  $B, T$  phase diagram from magnetostriction  $\Delta c/c$  vs field (black and red symbols), thermal expansion  $\Delta c/c$  vs temperature (blue symbol), and magneto-Raman measurements (open circles). Note that only lines above  $T = 1.5 \text{ K}$  are displayed due to the base temperature of our  $^4\text{He}$  fridge.

The energies of four phonon modes involving the Cu-O bonds vary monotonically with the magnetic field up to about 27 T. Around 20 T a change of slope is visible on the  $200 \text{ cm}^{-1}$  mode that can be associated with the closing of the spin gap in this system [8]. At higher fields, however, in addition to the phonon energy shifts, several anomalies were observed in the phonon energy as function of magnetic field. These anomalies are seen most clearly in the field dependence of the strongest pantograph mode at  $200 \text{ cm}^{-1}$  featuring the largest overall response to magnetic field and temperature [see Fig. 6(a)]. There are two kinks observed around  $\simeq 28 \text{ T}$  and  $\simeq 39 \text{ T}$  (also detected in  $450 \text{ cm}^{-1}$  and  $478 \text{ cm}^{-1}$  modes) that coincide with the kinks or plateaus observed in the magnetostriction measurements as shown in Figs. 6(b) and 7. There is also a more subtle anomaly manifesting as a change of slope at  $\simeq 34\text{--}35 \text{ T}$  similar to that detected in  $c$ -axis magnetostriction.

The magnetostriction  $\Delta c/c$  vs  $B$  and thermal expansion  $\Delta c/c$  vs  $T$  were measured at constant temperatures between 1.7 K and 14 K on the same crystal used for Raman experiment. From these experiments, it can be seen in Fig. 7 that the  $c$ -axis lattice parameter expands with fields monotonically, consistent with earlier results obtained in pulsed magnetic fields [8], and displays clearly seen plateaus corresponding to  $M/M_s = 1/4$  and  $1/3$ . Thermal expansion shown in Fig. 7 (top-left inset) was obtained that shows a large anomaly at the ordering temperature for the  $M/M_s = 1/3$  stripe phase. Combined magnetostriction, thermal expansion, and Raman scattering data was used to build the phase diagram displayed in Fig. 7 (bottom-right inset). Note that only lines above  $T = 1.5 \text{ K}$  are displayed due to the base temperature of our  $^4\text{He}$  fridge. The data amount to evidence supporting true bulk thermodynamic states for the stripe phases in  $\text{SrCu}_2(\text{BO}_3)_2$ .

Additionally, a curious phenomenon is seen in the magnetostriction curves, which appear to cross in the region of transition between  $M/M_s = 1/5$  and  $2/9$  stripe phases [8], suggesting an unusual vanishing and a change of sign of the coefficient of thermal expansion. Such change of sign has been seen in systems that display a divergence of the Grüneisen parameter [defined as the coefficient of thermal expansion  $\alpha$  divided by the specific heat  $C(T)$  at zero temperature] in the proximity of a quantum critical point (see Weickert *et al.* [34]). A full investigation requires access to lower temperatures and complementary measurements of the specific heat  $C(T)$ , and is currently under course.

## V. DISCUSSION

We have shown the results of expanding the range of magnetic fields in a magneto-Raman experiment to follow the magnetic field dependence of phonon modes involving Cu-O bonds of  $\text{SrCu}_2(\text{BO}_3)_2$  to magnetic fields high enough to reach the magnetic superstructures at  $M/M_s = 1/8$ ,  $1/4$ , and  $1/3$  that can shed light on the role of the lattice stabilizing magnetic structures and exotic spin states. We use density functional theory to successfully model and compute the energies of these modes, classifying them into two types: *pantograph* ( $200\text{ cm}^{-1}$  and  $450\text{ cm}^{-1}$ ) and *non-pantograph* ( $385\text{ cm}^{-1}$  and  $478\text{ cm}^{-1}$ ) modes. These four phonon modes exhibit unusual shifts at low temperatures below approximately 15 K while other phonon energies remain unaffected.

We show that all four modes are affected by the external magnetic field (applied along  $c$  axes) consistently with their

respective temperature dependencies; e.g., pantograph modes that are hardened with increasing temperature also harden with applied magnetic fields and nonpantograph modes that become softer with temperature also soften with applied fields and are, likely, going to be important in field- (or pressure-) induced states. We compare their field dependence against static physical properties (magnetization and magnetostriction). The detailed evolution of the mode energies in magnetic fields mimics the changes observed in dilatometry and magnetization to 45 T, displaying anomalies at plateaus. In particular, the field dependence of the strongest pantograph  $200\text{ cm}^{-1}$  mode and  $c$ -axis magnetostriction exhibit a striking resemblance with kinks at  $M/M_s = 1/8$  and  $1/3$  and slope change at  $M/M_s = 1/4$ . These strong magnetoelastic couplings revealed under temperature and magnetic field allow the use of combined dilatometry and Raman data to build a ( $B$  vs  $T$ ) phase diagram (see inset in Fig. 7) in good agreement with available data in the literature.

## ACKNOWLEDGMENTS

Z.L. and D.S. acknowledge support from the U.S. Department of Energy (Grant No. DE-FG02-07ER46451) for magneto-Raman measurements performed at the NHMFL, which is supported by NSF through Grant No. NSF/DMR-1644779 and the State of Florida. M.J. acknowledges support by DOE Office of Science BES project “Science at 100 Tesla.” B.D.G. acknowledges support from NSERC (Canada). This work was supported by HFML-RU/NWO-I, member of the European Magnetic Field Laboratory (EMFL).

- 
- [1] B. S. Shastry and B. Sutherland, *Physica B+C* **108**, 1069 (1981).
  - [2] D. I. Badrtdinov, A. A. Tsirlin, V. V. Mazurenko, and F. Mila, *Phys. Rev. B* **101**, 224424 (2020).
  - [3] H. Kageyama, K. Yoshimura, R. Stern, N. V. Mushnikov, K. Onizuka, M. Kato, K. Kosuge, C. P. Slichter, T. Goto, and Y. Ueda, *Phys. Rev. Lett.* **82**, 3168 (1999).
  - [4] S. Miyahara and K. Ueda, *Phys. Rev. Lett.* **82**, 3701 (1999).
  - [5] K. Kodama, M. Takigawa, M. Horvatić, C. Berthier, H. Kageyama, Y. Ueda, S. Miyahara, F. Becca, and F. Mila, *Science* **298**, 395 (2002).
  - [6] P. Sengupta and C. D. Batista, *Phys. Rev. Lett.* **98**, 227201 (2007).
  - [7] S. E. Sebastian, N. Harrison, P. Sengupta, C. D. Batista, S. Francoual, E. Palm, T. Murphy, N. Marcano, H. A. Dabkowska, and B. D. Gaulin, *Proc. Natl. Acad. Sci. USA* **105**, 20157 (2008).
  - [8] M. Jaime, R. Daou, S. A. Crooker, F. Weickert, A. Uchida, A. E. Feiguin, C. D. Batista, H. A. Dabkowska, and B. D. Gaulin, *Proc. Natl. Acad. Sci. USA* **109**, 12404 (2012).
  - [9] Y. H. Matsuda, N. Abe, S. Takeyama, H. Kageyama, P. Corboz, A. Honecker, S. R. Manmana, G. R. Foltin, K. P. Schmidt, and F. Mila, *Phys. Rev. Lett.* **111**, 137204 (2013).
  - [10] G. Radtke, A. Saúl, H. A. Dabkowska, M. B. Salamon, and M. Jaime, *Proc. Natl. Acad. Sci. USA* **112**, 1971 (2015).
  - [11] J. Romhányi, K. Penc, and R. Ganesh, *Nat. Commun.* **6**, 6805 (2015).
  - [12] S. Haravifard, D. Graf, A. E. Feiguin, C. D. Batista, J. C. Lang, D. M. Silevitch, G. Srajer, B. D. Gaulin, H. A. Dabkowska, and T. F. Rosenbaum, *Nat. Commun.* **7**, 11956 (2016).
  - [13] Z. Shi, W. Steinhardt, D. Graf, P. Corboz, F. Weickert, N. Harrison, M. Jaime, C. Marjerrison, H. A. Dabkowska, F. Mila, and S. Haravifard, *Nat. Commun.* **10**, 2439 (2019).
  - [14] D. Bhowmick and P. Sengupta, *Phys. Rev. B* **104**, 085121 (2021).
  - [15] J. Yang, A. W. Sandvik, and L. Wang, *Phys. Rev. B* **105**, L060409 (2022).
  - [16] Z. Shi, S. Dissanayake, P. Corboz, W. Steinhardt, D. Graf, D. M. Silevitch, H. A. Dabkowska, T. F. Rosenbaum, F. Mila, and S. Haravifard, *Nat. Commun.* **13**, 2301 (2022).
  - [17] K. Momma and F. Izumi, *J. Appl. Cryst.* **44**, 1272 (2011).
  - [18] S. Bettler, L. Stoppel, Z. Yan, S. Gvasaliya, and A. Zheludev, *Phys. Rev. Res.* **2**, 012010(R) (2020).
  - [19] P. Lemmens, M. Grove, M. Fischer, G. Güntherodt, V. N. Kotov, H. Kageyama, K. Onizuka, and Y. Ueda, *Phys. Rev. Lett.* **85**, 2605 (2000).
  - [20] K. Sparta, G. Redhammer, P. Roussel, G. Heger, G. Roth, P. Lemmens, A. Ionescu, M. Grove, G. Güntherodt, F. Hüning, H. Lueken, H. Kageyama, K. Onizuka, and Y. Ueda, *Eur. Phys. J. B* **19**, 507 (2001).

- [21] P. Lemmens, G. Güntherodt, and C. Gros, *Phys. Rep.* **375**, 1 (2003).
- [22] K.-Y. Choi, Y. G. Pashkevich, K. V. Lamonova, H. Kageyama, Y. Ueda, and P. Lemmens, *Phys. Rev. B* **68**, 104418 (2003).
- [23] A. Gozar and G. Blumberg, in *Frontiers in Magnetic Materials* (Springer-Verlag, Berlin/Heidelberg, 2015), pp. 735–754.
- [24] A. Gozar, B. S. Dennis, H. Kageyama, and G. Blumberg, *Phys. Rev. B* **72**, 064405 (2005).
- [25] C. C. Homes, S. V. Dordevic, A. Gozar, G. Blumberg, T. Rõõm, D. Hüvonen, U. Nagel, A. D. LaForge, D. N. Basov, and H. Kageyama, *Phys. Rev. B* **79**, 125101 (2009).
- [26] D. Wulferding, Y. Choi, S. Lee, M. Prosnikov, Y. Gallais, P. Lemmens, C. Zhong, H. Kageyama, and K.-Y. Choi, *npj Quantum Mater.* **6**, 102 (2021).
- [27] H. A. Dabkowska, A. B. Dabkowski, G. Luke, S. Dunsiger, S. Haravifard, M. Cecchinell, and B. D. Gaulin, *J. Cryst. Growth* **306**, 123 (2007).
- [28] M. Jaime, C. Corvalán Moya, F. Weickert, V. Zapf, F. F. Balakirev, M. Wartenbe, P. F. S. Rosa, J. B. Betts, G. Rodriguez, S. A. Crooker, and R. Daou, *Sensors* **17**, 2572 (2017).
- [29] P. Giannozzi, S. Baroni, N. Bonini, M. Calandra, R. Car, C. Cavazzoni, D. Ceresoli, G. L. Chiarotti, M. Cococcioni, I. Dabo, A. Dal Corso, S. de Gironcoli, S. Fabris, G. Fratesi, R. Gebauer, U. Gerstmann, C. Gougoussis, A. Kokalj, M. Lazzeri, L. Martin-Samos, N. Marzari, F. Mauri, R. Mazzarello, S. Paolini, A. Pasquarello, L. Paulatto, C. Sbraccia, S. Scandolo, G. Sclauzero, A. P. Seitsonen, A. Smogunov, P. Umari, and R. M. Wentzcovitch, *J. Phys.: Condens. Matter* **21**, 395502 (2009).
- [30] J. P. Perdew, K. Burke, and M. Ernzerhof, *Phys. Rev. Lett.* **77**, 3865 (1996).
- [31] M. Cococcioni and S. de Gironcoli, *Phys. Rev. B* **71**, 035105 (2005).
- [32] A. Togo and I. Tanaka, *Scr. Mater.* **108**, 1 (2015).
- [33] C. Vecchini, O. Adamopoulos, L. Chapon, A. Lappas, H. Kageyama, Y. Ueda, and A. Zorko, *J. Solid State Chem.* **182**, 3275 (2009).
- [34] F. Weickert, R. Küchler, A. Steppke, L. Pedrero, M. Nicklas, M. Brando, F. Steglich, M. Jaime, V. S. Zapf, A. Paduan-Filho, K. A. Al-Hassanieh, C. D. Batista, and P. Sengupta, *Phys. Rev. B* **85**, 184408 (2012).